ぐ ん ま 天 体 力 学 N 体 力 学 研 究 会

9-12 Mar. 2005, 群馬県立ぐんま天文台

メインベルト微小小惑星のサイズ頻度分布

Size Distribution of Small Main-Belt Asteroids as a Source of Near-Earth Asteroids

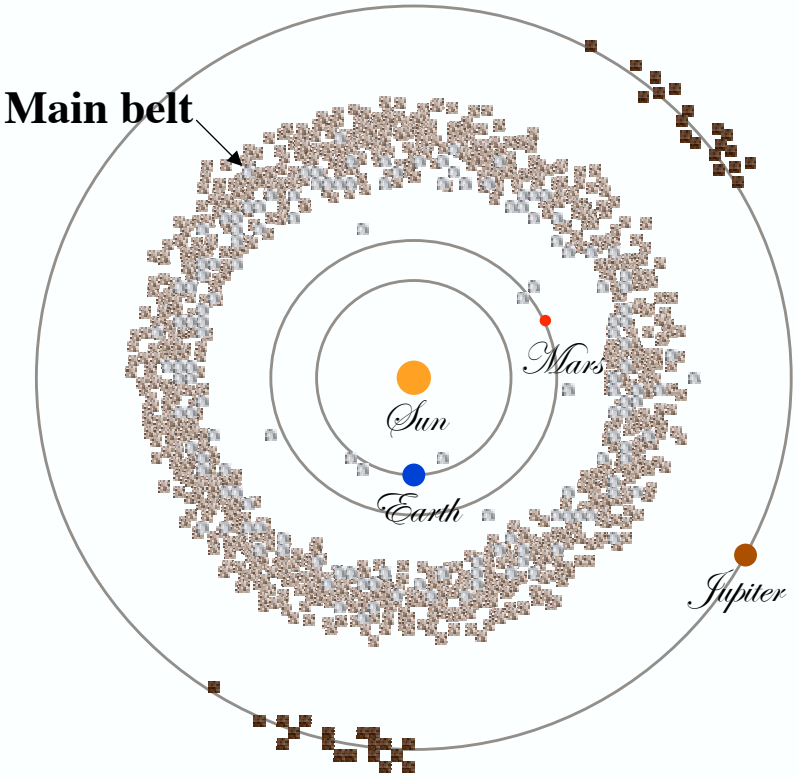

吉田二美・中村士

Fumi Yoshida (yoshdafm@cc.nao.ac.jp)

国立天文台

Based on data collected at Subaru Telescope which is operated by the National Astronomical Observatory of Japan.

Abstract

It has been proved dynamically that Near-Earth Asteroids (NEAs) originate from small members of the Main-Belt Asteroids (MBAs). However, this has not been confirmed yet observationally, because of the faintness of the source objects of NEAs. So, we used one of largest telescopes: the 8.2m Subaru Telescope and a wide field CCD camera: the Suprime-Cam, then we detected a large number of the small MBAs having the same size-range with NEA population. In this paper, under the hypothesis that the physical properties of NEAs should reflect those of the source objects, we compared directly the physical properties (taxonomic type and size distribution) between the NEAs and small MBAs.

Our observations was performed in 2001 October 21 (UT) with the R- and B-bands, the limiting magnitude was ~ 24.5 mag with the both bands. About 1000 MBAs were detected with the absolute magnitude (H) range of 13.6 < H < 23.0. We divided the detected asteroids into two groups, S- and C- type groups based on the B-R color of each asteroid.

We found that the ratio of S- to C-type in the surface density of MBAs varies from 3:2 in the inner-belt, 3:7 in the middle-belt, to 1:4 in the outer-belt. Basically the C-type asteroids dominated in the main-belt. We also found that the size distributions of the S- and C-type asteroids are similar with each other at the faint end: D < 1 km, their Cumulative Size Distribution (CSD) slopes (b) (i.e. N(> D) 宛 D^-b) were obtained as: b ~ 1.3. While the size distributions of larger asteroids (D > 1 km) seem to be different: the bs were 1.8 for the S-type and 1.3 for the C-type, respectively. Considering the large fraction of S-type asteroids in the NEA population comparing with the MBA population (e.g. Binzel et al. 2002), the source of NEA population should be the inner-belt asteroids because of the large fraction of S-type asteroids in there. There is an inconsistency on the size distributions between the NEAs population and S-type MBAs in the inner-belt. There must be some selection mechanisms on the transportation phase from the main-belt to near Earth region (e.g. Yarkovsky effect).

Our data on small MBAs can be the base in the study on a quantitative evaluation of the dynamical evolution of NEAs.

1. Introduction

So far about 3000 NEAs have been discovered by eager surveys. The physical properties of NEAs have been revealed gradually, for examples, (1) the average size of NEAs are remarkably smaller than that of MBAs ; (2) the S-type asteroids dominate in NEA population comparing with MBA population, even after applying observational bias-correction (Binzel et al. 2002, Stuart and Binzel 2004); (3) the slope index (b) of the Cumulative Size Distribution (hereafter CSD) (N(>D) 宛 D^-b) of NEAs is 1.95 at the range of 14 < H < 18.5 (Stuart 2001) or 1.75 at the range of 15 < H < 22 (Bottke et al. 2000)); (4) there are several very fast rotators in NEAs group. It has been predicted by several theoretical studies that the main source of NEAs seems to be small MBAs. However, it has not been confirmed observationally yet, because the small MBAs are very faint and past asteroid surveys with the small or middle class telescopes have not reached to the small MBAs population which has the same size-range with that of NEAs population. However, the 8.2 m Subaru Telescope which equipped with the wide field CCD camera: the Suprime-Cam are now available. This observation system allows us to detect a large number of small asteroids in the main-belt in a single wide field of view and examine the physical properties of the huge number of asteroids at the same time. This paper is a first one to investigate the source of NEAs by direct detection of the NEAs-sized MBAs. Since the taxonomic type determination of each asteroid is important to estimate the asteroid size, we measured the B-R color of each asteroid. Although the strict classification of asteroids into several taxonomic types is impossible by only their B-R color as you will see in Fig.5, we can divide roughly asteroids into two groups by the B-R: i.e. S- and C-types which they are main components of MBAs. If the main source of NEA population is truly the small MBA population, the physical properties (e.g. taxonomic type and size distribution) should be similar with each other under the assumption that NEAs have not been undergoing any physical or chemical evolutions during the transportation from the main-belt to near Earth region. Under this assumption, we compared the size and taxonomic distributions of NEAs with those of our detected asteroids.

2. Observations and Data Reduction

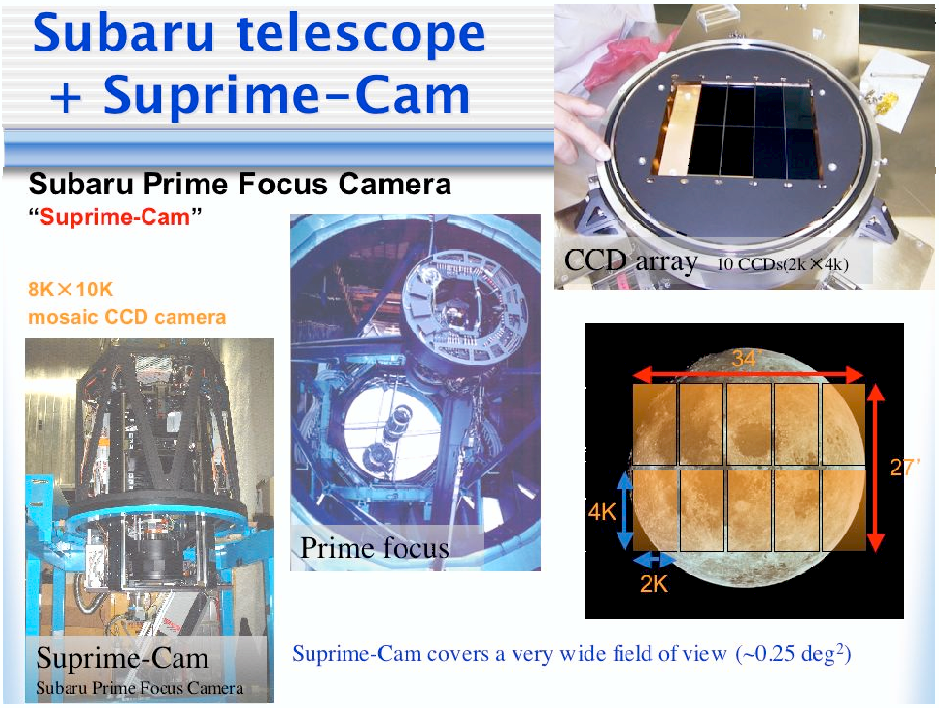

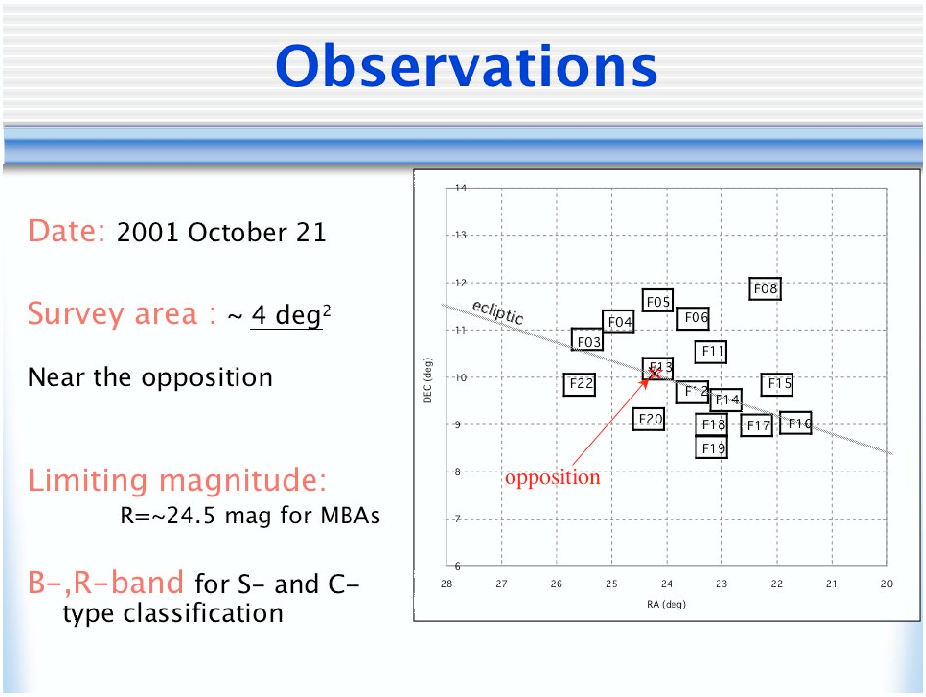

Our observation was carried out on 2001 October 21 (UT). We used the 8.2 m Subaru telescope at atop of Mauna Kea in Hawaii, which was equipped with the Suprime-Cam to the primefocus. Image reduction was performed using the standard method with IRAF. First, the average value of the overscan region of each CCD was subtracted from each CCD image data. Second, the images of each band were Dflat-fielded by dividing them by a median dome flat at each band. Next we made the composition images of each field by using three images to detect moving objects: i.e. the B-band image was

added to the first R-band image and then the second R-band image was subtracted from it. After this procedure, moving objects appear along a line as a trio of white-white-black dots on the combined images (see Fig. 1). With careful eye-inspection for all the composite images, we found 1838 moving objects in the 16 fields (table 1). After we detected the moving objects, we measured their motion and brightness by using IRAF APPHOT package on the single image. For the measured magnitude of each moving object, a correction of the atmospheric extinction was applied by using the Landolt standard stars. And also a correction of chip-by-chip sensitivity difference was done by comparing counts of the sky background brightness of the object image to 10 ccd chips.

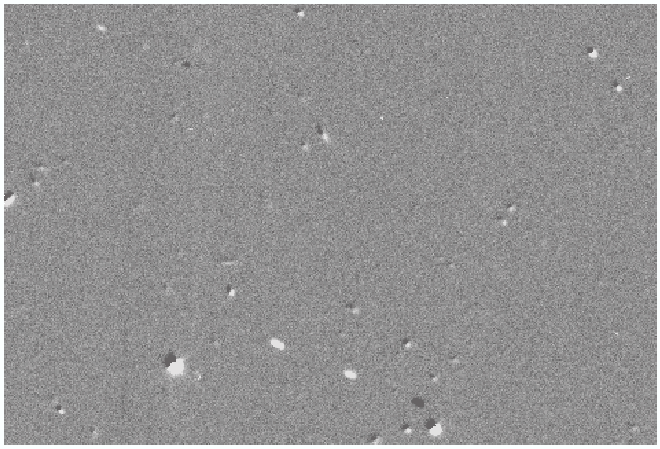

Fig. 1. Moving objects on the combined image. One can see two moving objects in this image (one object is at the upper left and another one is at the bottom of middle). The stars slightly shifted on the combined images because of the error of the telescope pointing. This image is a part of one CCD image, its field of view is 1.5 × 1 square arcminutes.

Table 1 Observational log and the detection number of moving objects

Field	No.	Filter	UT-start	Airmass			CCD							total
					0	1	2	3	4	5	6	7	8	9	
F03	1	R	13:00:21.1	1.358	9	11	8	9	12	20	13	15	14	15	126
F03	2	B	13:20:32.8	1.511											
F03	3	R	13:41:17.0	1.579											
F04	1	R	12:56:24.1	1.375	9	7	10	21	18	13	9	15	13	9	122
F04	2	B	13:16:36.2	1.426											
F04	3	R	13:37:24.6	1.550											
F05	1	R	12:34:54.3	1.177	9	23	9	10	5	13	14	11	10	15	118
F05	2	B	12:54:49.1	1.244											
F05	3	R	13:14:41.9	1.337											
F06	1	R	11:56:47.0	1.153	11	17	14	15	8	17	12	16	10	12	132
F06	2	B	12:17:06.3	1.236											
F06	3	R	12:37:01.4	1.336											
F08	1	R	08:47:17.0	1.045	10	5	7	10	11	14	11	13	8	8	97
F08	2	B	09:07:37.5	1.036											
F08	3	R	09:27:20.1	1.044											
F11	1	R	11:13:37.0	1.078	13	10	8	13	9	8	9	8	9	12	101
F11	2	B	11:33:38.9	1.113											
F11	3	R	11:53:50.2	1.158											
F12	1	R	12:00:53.4	1.151	12	19	18	8	16	12	12	11	12	7	127
F12	2	B	12:20:51.2	1.248											
F12	3	R	12:40:54.0	1.333											
F13	1	R	12:08:51.3	1.136	16	13	19	13	13	11	11	15	13	12	133
F13	2	B	12:28:48.9	1.257											
F13	3	R	12:48:34.2	1.356											
F14	1	R	11:01:43.6	1.052	9	12	13	16	7	7	11	15	11	14	115
F14	2	B	11:21:01.9	1.085											
F14	3	R	11:41:25.9	1.136											

Field	No.	Filter	UT-start	Airmass			CCD							total
					0	1	2	3	4	5	6	7	8	9	
F15	1	R	08:43:20.9	1.055	8	7	10	5	6	14	13	19	7	6	92
F15	2	B	09:03:42.1	1.034											
F15	3	R	09:23:21.3	1.021											
F16	1	R	08:39:30.6	1.061	13	12	13	18	11	16	9	9	8	9	118
F16	2	B	08:59:42.4	1.039											
F16	3	R	09:19:32.9	1.025											
F17	1	R	08:51:21.1	1.050	6	9	8	10	8	12	11	9	13	6	92
F17	2	B	09:11:21.0	1.032											
F17	3	R	09:31:18.2	1.021											
F18	1	R	11:05:40.3	1.068	11	9	17	17	8	18	10	13	13	10	126
F18	2	B	11:25:18.0	1.102											
F18	3	R	11:45:12.3	1.145											
F19	1	R	11:09:50.5	1.077	9	11	10	12	11	12	7	24	9	10	115
F19	2	B	11:29:43.9	1.112											
F19	3	R	11:48:60.0	1.157											
F20	1	R	12:52:31.0	1.380	7	13	6	10	9	11	6	3	9	11	85
F20	2	B	13:12:39.4	1.503											
F20	3	R	13:33:31.1	1.668											
F22	1	R	13.04.10.2	1.412	9	8	16	14	16	17	17	12	12	18	139
F23	2	B	13:24:27.0	1.544											
F23	3	R	13:45:27.1	1.796											
			total		158	186	186	201	166	215	175	206	171	174	1838

In order to estimate the detectable limiting magnitude of MBAs at the each observing field, we used artificial objects which mimic the image of the actual inner-belt MBAs. At first, we made 80 artificial object trails with offset by magnitude difference of 0.2 mag by using the IRAF MKOBJECTS package and then put them on the combined image which we used to detect moving objects. We detected the artificial objects by eye-inspection, then we counted the number of objects detected at each magnitude. We defined the 90 %-detection-magnitude of the lowest detection efficiency as a limiting magnitude in this survey. The MBAs move with the rate of 1.17, 1.04, and 0.92 arcsec during the exposure (2 minutes) at a=2.6 AU, 3.0 AU, and 3.5 AU, respectively. The mean seeing size on our observing night was ~ 0.8 arcsec. Trailing loss effect was explored by the different length of the artificial trails.

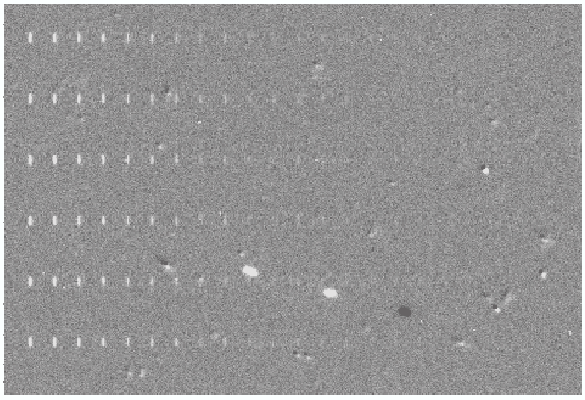

Fig. 2. Artificial trails on the combined image.

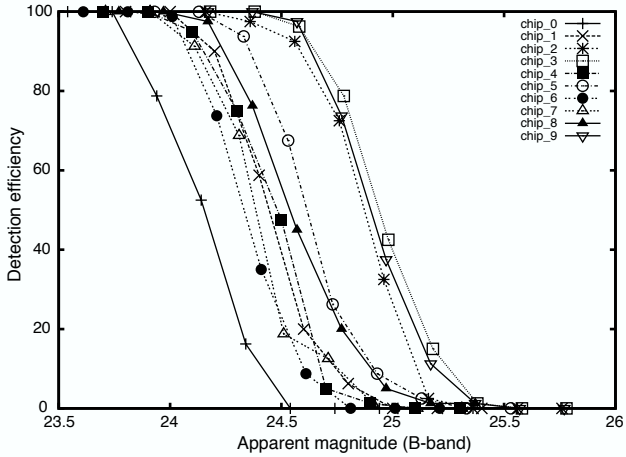

Fig. 3. Detection efficiency of the artificial trails

Table 2 Limiting magnitude for MBAs in our survey

Region of main-belt	Apparent magnitude R-band	Apparent magnitude B-band	Absolute* magnitude	Diameter (km)** S-type	Diameter (km)** C-type
Inner ($2.0 \leq a(\mathrm{AU}) < 2.6$)	23.90	23.85	21.25	0.16	0.32
Middle ($2.6 \leq a(\mathrm{AU}) < 3.0$)	24.05	24.08	20.61	0.21	0.43
Outer ($3.0 \leq a(\mathrm{AU}) < 3.5$)	24.21	24.25	19.95	0.29	0.58

**We calculated the absolute magnitude H at V-band by using the mean V-R value of the known S-type and C-type asteroids.*

***We converted from the absolute magnitude to the diameter by using the mean V-R value and the mean albedo each S- and C-type group, respectively. See text for more detail in subsection 3.3.*

3. Identification of MBAs

3.1. Estimation of Semi-major axis and Inclination for Each Moving Object

The apparent velocities of 1734 objects among 1838 detected objects were measured.

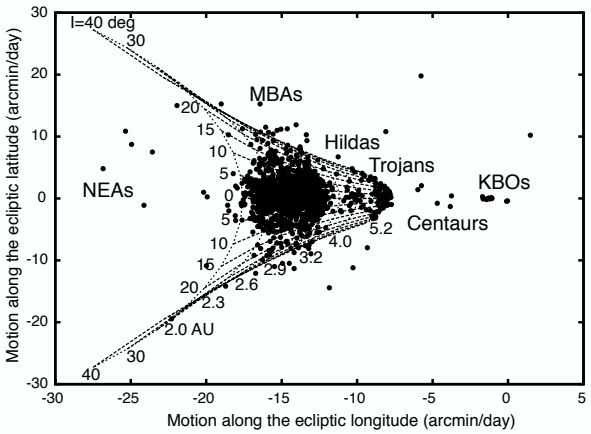

Fig. 4. Apparent motions of moving objects. One can see the moving objects divided into several groups of the various populations.

$$a = \frac{1}{2\gamma}\left(\gamma - 2k\lambda \pm \sqrt{|\kappa|}\right), \quad (1)$$

$$\tan I = \frac{|\beta|}{\lambda + \frac{k}{a-1}}, \quad (2)$$

$$\gamma = \lambda^2 + \beta^2, \quad (3)$$

$$\kappa = \gamma^2 - 4k\lambda\gamma - 4k^2\beta^2, \quad (4)$$

Lines in Fig. 4 show the motion of the moving object whose the orbital eccentricity (e) are zero at various semi-major axis (a) and inclination (I) at opposition. We chose 1001 objects within a = 2.0-3.5 AU and I = ±40 degrees as MBAs. When we detect asteroids near oppositions, we can calculate approximately the a and I of each asteroid from its apparent motion assuming its e = 0 by using the Bowell's equations. The a and I obtained by the equations include the errors of ~ 0.1 AU and 1 ~ 5 degrees, respectively, because the e is actually not zero (0.1 ~ 0.2) for real asteroids (Bowell et al. 1990; Nakamura & Yoshida, 2002; Yoshida et al. 2003). The error on the a would bring an uncertainty of ~ 20% to asteroid diameter.

Absolute magnitude distribution

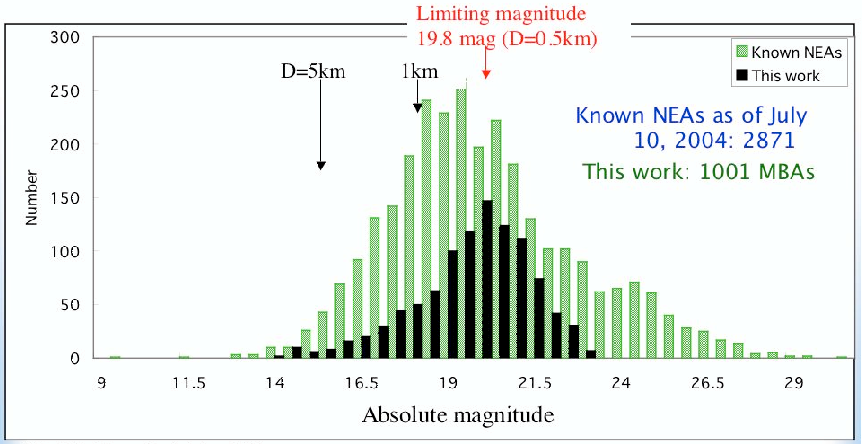

H=V-5log{a×(a-1)}

←The absolute magnitude distribution of detected asteroids by Subaru.

3.2. Estimation of Taxonomic Type

The S- and C-type asteroids seem to be classified by their B-R and/or V-I colors based on the known MBAs data (PDS Asteroid DataArchive, <http://www.psi.edu/pds/archive/ecas.html>,<http://www.psi.edu/pds/archive/tax.html>). As we mentioned in the introduction, since this survey is related to the origin of NEAs, it is important to distinguish between the S- and C-type asteroids in order to investigate the source region of the S-type asteroids among the NEAs population. Moreover, the diameter of the C-type asteroid with a certain brightness is two times larger than that of the S-type one with the same brightness, because of the difference of their albedos. Thus, for estimating accurate asteroid size, the S- and C-type asteroids must be divided.

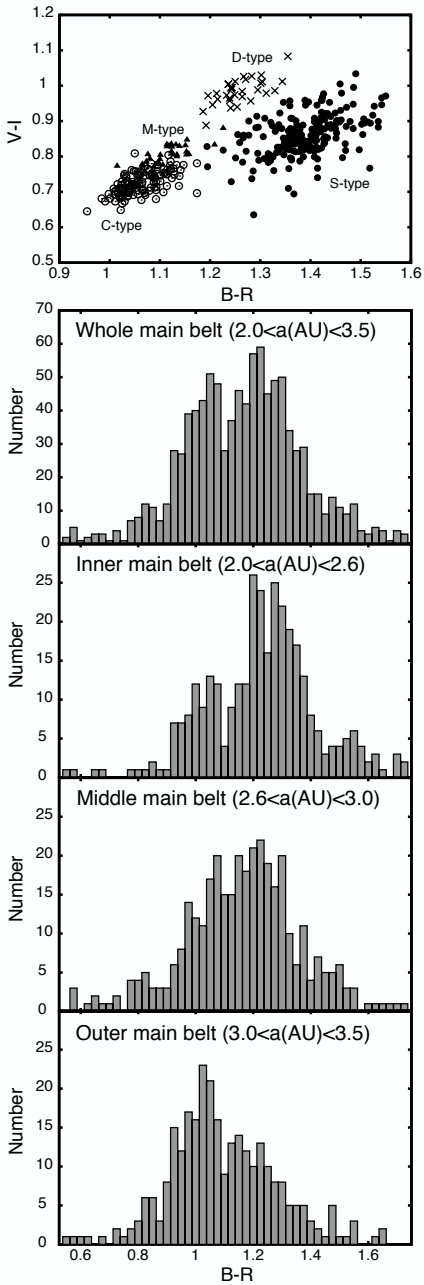

Fig. 5. Colors of know asteroids (the top panel) and the B-R color of asteroids detected in this survey (the last four panels). In the top panel, one can see that the S, C, D, and M-types are splitted on the B-R vs. V-I diagram. The last four panels show the histograms of the B-R colors of our asteroids for different main-belt regions.

3.3. Estimation of Asteroid Size

The asteroid diameter (D) is calculated based on its albedo (p) and its H by the following equation.

$$\log D = 3.1295 - 0.5 \log p - 0.2 H \qquad (5)$$

We used the mean albedos obtained from the asteroids database "Small Bodies Node" (PDS Asteroid Data Archive, IRAS-A-FPA-3-RDR-IMPS-V4.0, <http://www.psi.edu/pds/archive/albedo.html>) for each S- and C-type group, namely, p = 0.21 for S-type asteroids and p = 0.06 for C-type asteroids, respectively. After we calculated the diameter of 1001 MBAs, it turned out that more than 80 % MBAs which we detected in this survey are smaller than 1 km in diameter.

4. Heliocentric Distribution of S- and C-type MBAs

(a) (c)

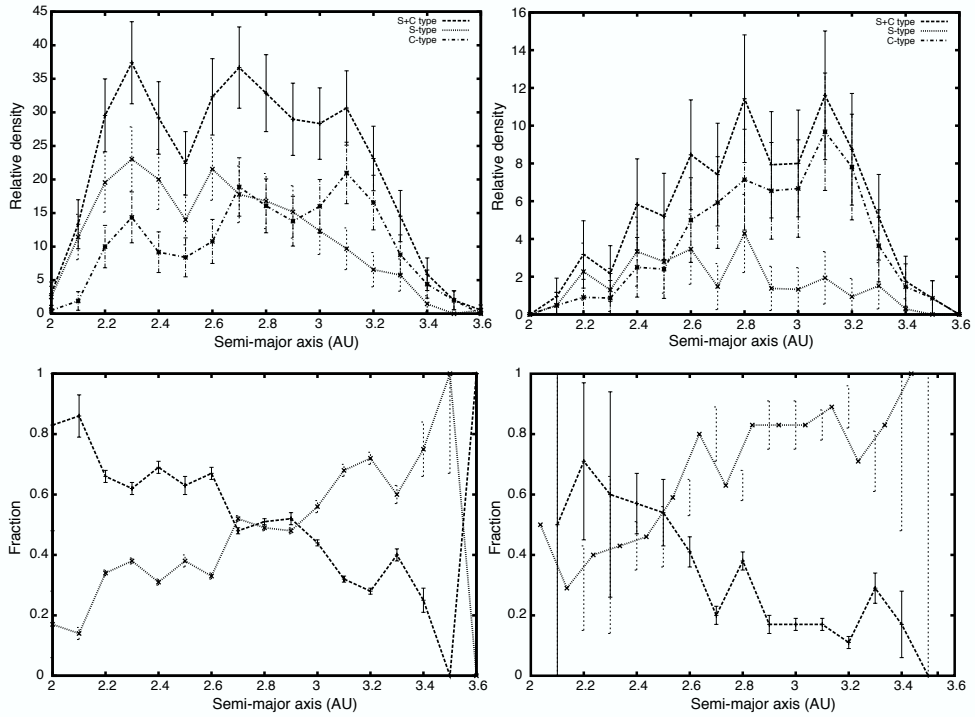

(b) (d)

Fig. 6 (a) and (b) show the observed surface density of asteroids and the fraction of each type to the total surface density as a function of heliocentric distance for 1001 MBAs. (c) and (d) are bias-corrected surface density and the fraction of both types, respectively.

One can see the depletion of asteroids around a = 2.5 AU and 2.8-3.0 AU in Fig. 6(a). These region are corresponding to the mean motion resonances (3:1, 5:2 or 7:3) with Jupiter. The S- and C-type asteroids are indicated by solid line and dot line, respectively. The distributions of two types asteroids are obviously different: the S-type asteroids dominate in the inner main-belt, the C-type asteroids dominate in the outer main-belt. Fig. 6 (a) and (b) include the observational bias so that we could not detect the faint asteroids in the outer region of main-belt and much more S-type asteroids are discovered at any limiting magnitude than C-type are, because of their high albedo. Taking account of such observational bias, we re-plotted these figures in Fig. 6 (c) and (d); (c): surface density and (d): fraction of each type by using the asteroids larger than 0.6 km which seems to be completed in our survey.

5. Size Distribution of S- and C-type MBAs

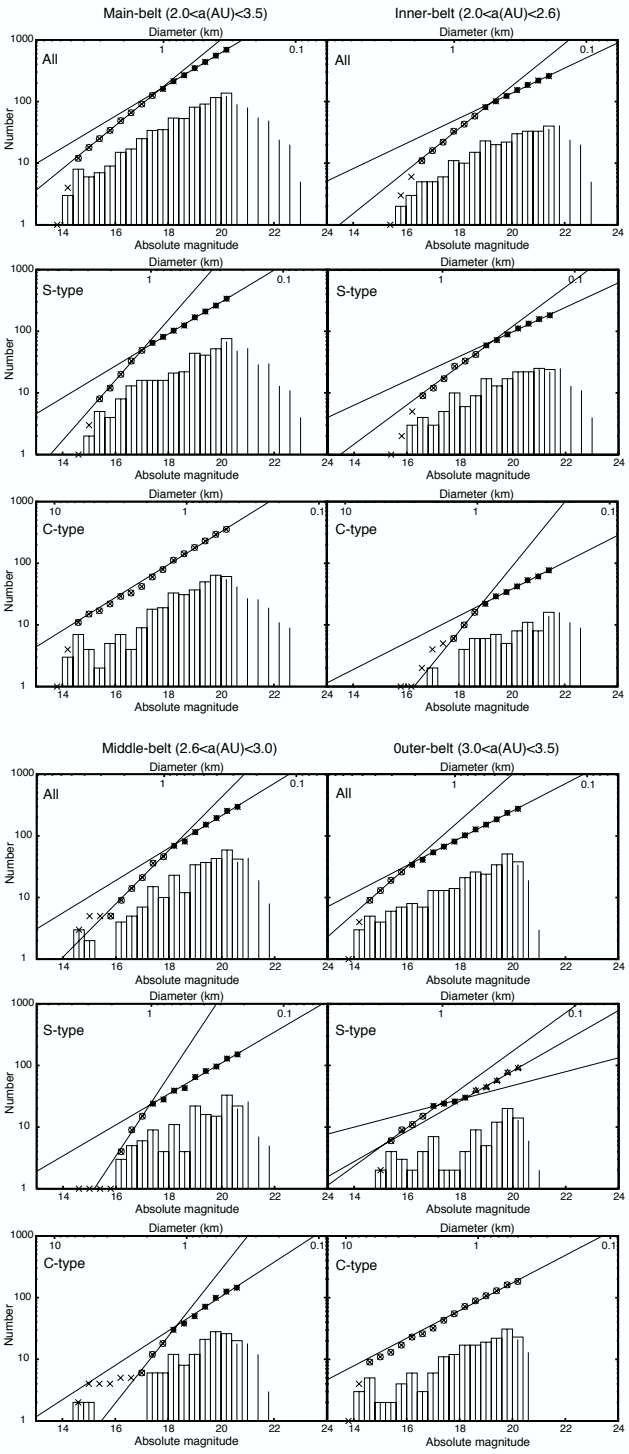

We investigated the size distributions of our MBAs for each type in the different main-belt regions: i.e. the whole-belt (2.0 < a(AU) < 3.5,), the inner-belt (2.0 < a < 2.6), the middle-belt (2.6 < a < 3.0), and the outer-belt (3.0 < a < 3.5) (Fig.7). We noticed that for small asteroids (D < 1 km), the CSD-slopes index of each type are similar with each other in any regions (the slopes were listed in table 3). Their slopes are 1.0-1.2 in the inner-belt and the outer belt. In the middle- belt, the slopes (1.3-1.4) are slightly larger than others. We reported before that the size distribution of asteroids may have differences between the inner-belt and outer-belt regions in our previous survey (Yoshida et al. 2003) as well as previous studies (e.g., Jedicke & Metcalfe 1998). However the Sloan Digital Sky Survey (SDSS) did not find any evidence that the size distribution varies with the heliocentric distance (Ivezi´c et al. 2001). Since all previous studies, except SDSS, assumed the mean albedo of asteroids because of the lack of their color information, despite significant differences in the mean albedo and heliocentric distribution on the major two different groups in the main-belt, we must think about the possibility that the mean albedo assumption brought apparent difference in the cumulative size distribution in the main-belt.

Fig.7 Size distributions of MBAs in the different regions in the main-belt.

In this new survey, we distinguished between S- and C-type, then we did not find that there is a clear difference of size distributions. However, Cheng (2004) mentioned that MBAs larger than 5 km in diameter are remnants which have survived over the collisional evolution in the main-belt until now. It is likely that the size distribution of planetesimals varies with the heliocentric distance in early solar system. We would like to keep getting more data and then confirm the size distribution differences.

Table 3 The CSD-slopes (b) in each main-belt region and each type asteroid. The fitting regions are shown in parentheses.

Types	Whole-belt	Inner-belt	Middle-belt	Outer-belt
S and C	1.29 ± 0.02	1.02 ± 0.03	1.31 ± 0.07	1.11 ± 0.02
	(17.8-20.2 mag)	(19.0-21.4 mag)	(18.2-20.6 mag)	(16.2-20.2 mag)
	1.75 ± 0.02	1.72 ± 0.06	2.16 ± 0.18	1.89 ± 0.07
	(14.6-17.4 mag)	(16.6-18.6 mag)	(15.8-17.8 mag)	(14.6-15.8 mag)
S-type	1.29 ± 0.02	0.99 ± 0.04	1.26 ± 0.05	1.22 ± 0.09
	(17.4-20.2 mag)	(19.0-21.4 mag)	(17.4-20.6 mag)	(18.6-20.2 mag)
	2.44 ± 0.09	1.59 ± 0.12	3.25 ± 0.44	0.56 ± 0.06
	(15.4-17.0 mag)	(16.6-18.6 mag)	(16.2-17.0 mag)	(17.0-18.2 mag)
				1.55 ± 0.13
				(15.4-16.6 mag)
C-type	1.33 ± 0.03	1.09 ± 0.03	1.39 ± 0.10	1.12 ± 0.03
	(14.6-20.2 mag)	(19.0-21.4 mag)	(18.2-20.6 mag)	(14.6-20.2 mag)
		2.63 ± 0.06	2.71 ± 0.44	
		(17.8-18.6 mag)	(17.0-17.8 mag)	

6. Spatial Distribution of S- and C-type MBAs

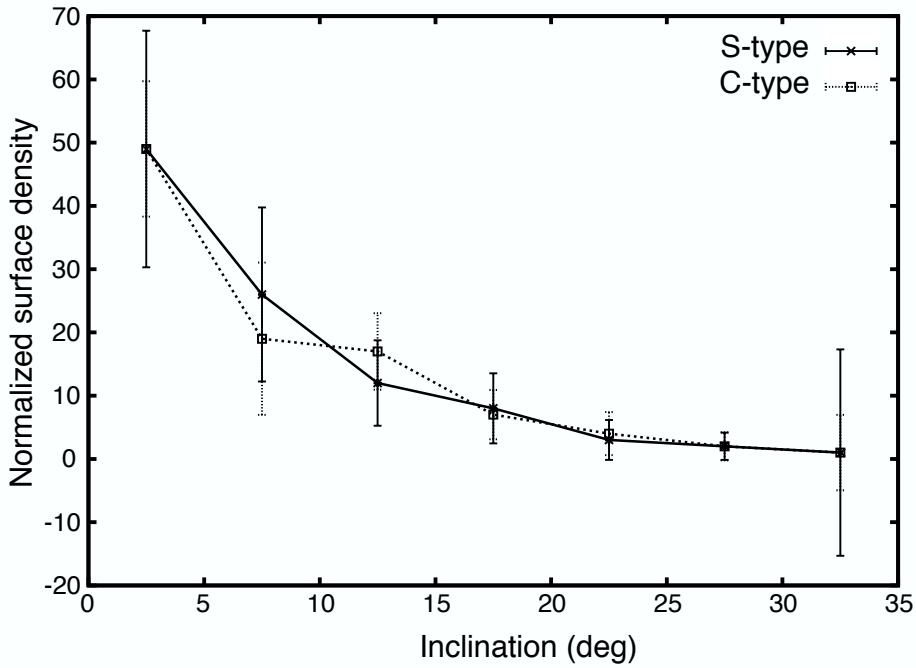

Fig. 8. The normalized surface density of the S- and C-type populations as a function of inclination.

We examined the spatial distributions along the ecliptic latitude of S- and C-type asteroids. We calculated the normalized surface density as a function of inclination as follows. At first we divided asteroids into the bins having the range of 0.2 AU in the a and 5 deg in the I, and then counted the number of asteroids in each bin, next calculated the percentage of the number of asteroids at each bin to the total number of asteroids including in the range of 0.2 AU in the a.

The solid line in Fig. 8 shows the normalized surface density of S- type population (517 asteroids) detected in the whole main-belt, the dotted line shows that of C-type population (484 asteroids). The error bars indicate the variation of the normalized surface density changing with the heliocentric distance. There is no significant difference of the distribution between S- and C-type. Asteroids of both types decrease exponentially with increasing their inclinations.

7. Summary and Discussion

The fraction of the S- to C-type asteroids from this survey varies with the heliocentric distance: for samples defined by the same absolute magnitude cutoff, the ratio of the S- to C-type asteroids changes from 4:1 at a ~ 2 AU, 1:1 at a ~ 2.8 AU, to about 3:7 at a = 3.0-3.4 AU (see figure 4 (a) (b)), for samples defined by the same size cutoff, namely for D > 0.6 km until which our survey is completed in the whole main-belt, the ratio of the S- to C-type asteroids is 3:2 in the inner main-belt, the ratio reverses around 2.5 AU, it becomes 1:4 in the outer main-belt (see figure 4 (c) (d)). The ratio of S- to C-type is 1:2.3 in the whole main-belt. These results are roughly consistent with the results obtained by the SDSS (Ivezi´c et al. 2001). Based on our estimation of size distribution of smaller MBAs (D < 1 km), we predict that the number fraction of the S- to C-type asteroids (1:2.3) would be invariable until much smaller MBAs (D ~ 0.1 km).

We estimated the size distribution in the entire main-belt for S-type population down to D = 0.29 km and for C-type population down to D = 0.58 km. The CSD-slopes of the asteroids smaller than 1 km in diameter are very close to ~ 1.3 for both types. This result is consistent with that of SDSS found the CSD-slope (1.3) for asteroids with the size range of 0.4 < D(km) < 5. However, for S-type asteroids larger than 1 km in diameter, the SDSS and our survey have an inconsistency, namely our CSD-slope is close to 2, the SDSS's CSD-slope is 1.2 (Ivezi´c et al. 2001). About 80 % asteroids detected in our survey are smaller than 1 km in diameter. The small sampling number of large S-type (D > 1 km) in our survey might induce the inconsistency.

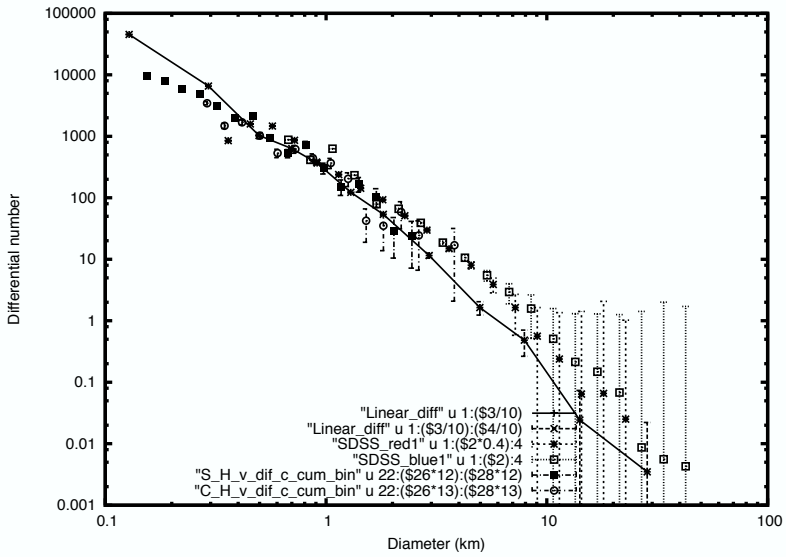

Fig. 9. Size distributions of LINEAR, SDSS, and our asteroid survey. The solid line shows the size distribution of NEAs from Stuart and Binzel (2004). The + and □ show the size distributions of the SDSS red (S-type) and SDSS blue (C-type), respectively. The ▪ and ◯ show the size distributions of our S-type and C-type asteroids in the inner-belt, respectively.

We compared our size distributions for both types with that of NEAs obtained by Stuart and Binzel (2004) and those of SDSS (Ivezi´c et al. 2001) in Fig.9. The solid line shows the differential size distribution of NEAs. The + and ▫ are the differential size distribution of SDSS S-type and C-type, ▪ and ◯ are our Subaru S-type and C-type asteroids in the inner-belt, respectively. Our survey extended the faint end of the SDSS down to 0.16 km in the inner-belt region. The slopes of the SDSS and ours are similar with each other. However, the shape of size distribution of NEAs seems to be different from those of the SDSS and ours in any size-ranges. Based on the excess of S-type asteroids in the NEAs population obtained from observations, if it is truly de-biased data, the large fraction of the S-type asteroids in the inner-belt obtained from our survey (Fig.6 (d)) must be an evidence that the NEAs population originate from the inner-belt region. However, when we compared the size distribution of NEAs with that of our S-type asteroids of the inner-belt and those of the SDSS, they are different from one another. This means that there must be some selection mechanisms for the transportation phase from the main-belt to near Earth region (e.g. Yarkovsky effect).

Our data of the small MBAs can be the base on the study on the dynamical evolution of NEAs. Especially, it would be a good data for estimating quantitatively the contribution of the Yarkovsky effect into the dynamical evolution of NEAs. At last, we show Fig. 10 including an interesting speculation about early Solar System. Dr. T. Ito will present several interesting evidence and speculation about this figure in his talk.

We thanks Z. Ivezi'c, J. Stuart and B. G. Strom for providing their data.

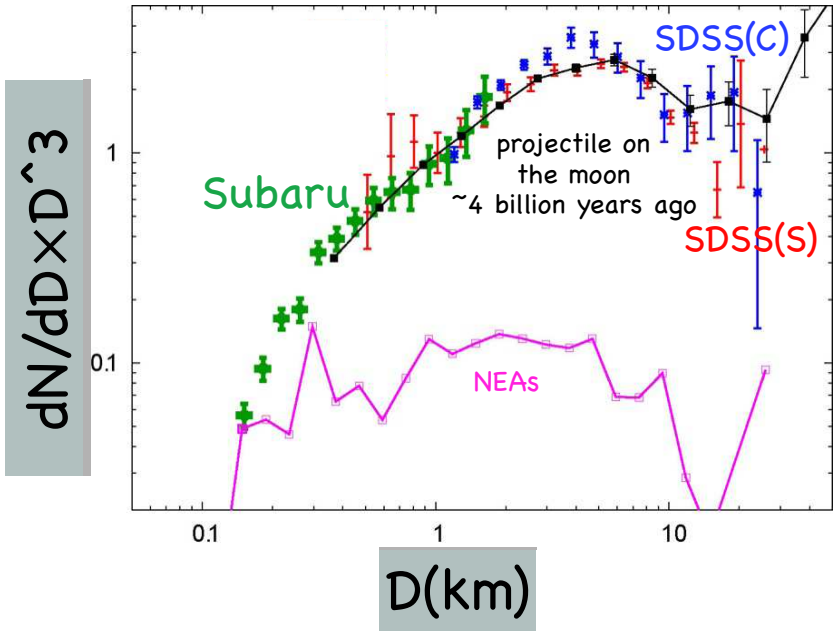

Fig.10. The current size distributions of MBAs (Subaru and SDSS) and NEAs comparing with that of the projectile which impacted on the moon ~ 4 billion years ago. The size distribution of MBAs does not change at all during 4 billion years until now ?

References

Binzel, R.P., Rivkin, A.S., Stuart, J.S., Harris, A.W., Bus S.J., and Burbine T.H. Observed spectral properties of near-Earth objects: results for population distribution, source regions, and space weathering processes. Icarus 170, 259-294, 2004.

Bottke, Jr., W.F., Jedicke, R., Morbidelli, A., Petit, J.M., and Gladman, B. Understanding the distribution of Near-Earth asteroids. Science 288, 2190-2194, 2000.

Bottke, Jr., W.F., Morbidelli, A., Jedicke, R., Petit, J.M., Levison, H.F., Michel P,. and Metcalfe, T.S. Debiased orbital and absolute magnitude distribution of near-Earth objects. Icarus 156, 399-433, 2002.

Bowell, E., Skiff, B.A., Wasserman, L.H., and Russell, K.S., in Asteroids, Comets, Meteors (Proc. of ACM 89 Meeting), ed. C. I. Lagerkvist, H. Rickman, & B. A. Lindblad (Uppsala: Uppsala University). Orbital Information from Asteroid Motion Vectors. 19-24, 1990.

Cheng A.F. Collisional evolution of the asteroid belt. Icarus 169, 357-372, 2004.

Davis D.R. On the size distributions of asteroid taxonomic classes: the collisional interpretation. in Asteroids, Comets, Meteors (Proc. of ACM 89 Meeting), ed. C. I. Lagerkvist, H. Rickman, & B. A. Lindblad (Uppsala: Uppsala University). Orbital Information from Asteroid Motion Vectors. 39-44, 1990.

Ivezi´c, Z., Tabachnik, S., Rafikov, R., Lupton, R.H., Quinn, T., Hammergren, M., Eyer, L., Chu, J., Armstrong, J.C., Fan, X., Finlator, K., Geballe, T.R., Gunn, J.E., Hennessy, G.S., Knapp, G.R., Leggett, S.K., Munn, J.A., Pier, J.R., Rockosi, C.M., Schneider, D.P., Strauss, M.A., Yanny, B., Brinkmann, J., Csabai, I., Hindsley, R.B., Kent, S., Lamb, D.Q., Margon, B., McKay, T.A., Smith, J.A., Waddel, P., and York D.G. (for the SDSS Collaboration) Solar system objects observed in the Sloan Digital Sky Survey commissioning data. The Astronomical Journal 122, 2749-2784, 2001.

Jedicke, R., and Metcalfe T.S. The orbital and absolute magnitude distributions of main belt asteroids. Icarus 131, 245-260, 1998.

Michel, P., Benz, W., and Richardson, D.C., Catastrophic disruption of preshattered parent bodies. Icarus 168, 420-432, 2004.

Miyazaki, S., Komiyama, Y., Sekiguchi, M., Okamura, S., Doi, M., Furusawa, H., Hamabe, M., Imi, K., Kimura, M., Nakata, F., Okada, N., Ouchi, M., Shimasaku, K., Yagi, M., and Yasuda, N. Subaru Prime Focus Camera-Suprime-Cam. Publications of the Astronomical Society of Japan 54, 833-853, 2002.

Morbidelli, A. Jedicke, R.,Bottke, W.F., Michel P,. and Tedesco, E.F. From magnitudes to diameters: the albedo distribution of near Earth objects and the Earth collision hazard. Icarus 158, 329-342, 2002.

Nakamura, T., and Yoshida, F. Statistical method for deriving spatial and size distributions of sub-km main-belt asteroids from their sky motions. Publications of the Astronomical Society of Japan 54, 1079-1089, 2002.

Rabinowitz, D., Helin, E., Lawrence, K., and Pravdo, S. A reduced estimate of the number of kilometre-sized near-Earth asteroids. Nature 403, 165-166.

Stuart, J.S. A Near-Earth Asteroids population estimate from the LINEAR survey. Science 294, 1691-1693, 2001.

Stuart J.S. and Binzel R.P. Bias-corrected population, size distribution, and impact hazard for the near-Earth objects. Icarus 170, 295-311, 2004.

Yoshida, F., Nakamura, T., Fuse, T., Komiyama, Y., Yagi, M., Miyazaki, S., Okamura, S., Ouchi, M., Miyazaki, M. First Subaru observations of sub-km main-belt asteroids. Publications of the Astronomical Society of Japan 53, L13-L16, 2001.

Yoshida, F., Nakamura, T., Watanabe, J., Kinoshita, D., Yamamoto, N., Fuse, T. Size and spatial distributions of sub-km main-belt asteroids. Publications of the Astronomical Society of Japan 55, 701-715, 2003.

Yoshida, F., and Nakamura, T. Basic nature of sub-km main-belt asteroids: their size and spatial distributions. Advances in Space Research 33, 1543-1547, 2004.